

Supporting Information

Structure-property-activity relationships in a pyridine containing azine-linked covalent organic framework for photocatalytic hydrogen evolution

*Frederik Haase,^{†‡} Tanmay Banerjee,[†] Gökcen Savascı,[†]
Christian Ochsenfeld[†] and Bettina V. Lotsch^{†‡§*}*

[†]Max Planck Institute for Solid State Research, Heisenbergstraße 1, 70569 Stuttgart, Germany

[‡]Department of Chemistry, University of Munich (LMU), Butenandtstraße 5-13, 81377
München, Germany

[§]Nanosystems Initiative Munich (NIM) & Center for Nanoscience, Schellingstraße 4, 80799
München, Germany

*To whom correspondence should be addressed. E-mail: b.lotsch@fkf.mpg.de

List of tables

Table S1: Parameters of Rietveld refinement	- 5 -
Table S2: Dihedral angles in PTP-CHO and N _x -CHO building blocks obtained from optimized geometries on the PBE0-D3/def2-TZVP level of theory. Dihedral angles are reported in a clockwise order, starting from the upward pointing ligand A. Structures of the respective aldehydes can be found in Figure 1.	- 5 -
Table S3: Radiative and non-radiative rates of PTP-COF under different experimental conditions...	- 5 -
Table S 4: Excitation energies for the PTP-CHO building block unit calculated on TD-PBE0/def2-TZVP level of theory.	- 6 -
Table S5: Calculated vertical radical stabilization energies as differences in total energies between radical anionic, radical cationic and neutral states of the PTP-CHO model system, PBE0-D3/def2-TZVP level of theory.	- 6 -

Table of figures

Figure S1: XRPD of PTP-COF synthesized in different solvent systems. DMAc = dimethyl acetamide, <i>o</i> -DCB = <i>o</i> -dichlorobenzene.....	- 7 -
Figure S2: Full IR Spectrum of PTP-CHO and PTP-COF.....	- 7 -
Figure S3: ^{13}C ssNMR of PTP-COF. Asterisks denote spinning side bands.....	- 8 -
Figure S4: Rietveld refinement of the PTP-COF shows a good fit to the experimentally observed powder pattern (Rwp : 1.833).....	- 8 -
Figure S5: BET fit of the surface area of PTP-COF.....	- 9 -
Figure S 6: SEM image of the PTP-COF showing the spherical particles and the intergrown agglomerates.....	- 9 -
Figure S7: Hydrogen evolution under full spectrum light.....	- 10 -
Figure S8: Spectrum of the xenon lamp with the dichroic mirror used for the AM1.5 photocatalysis experiments.....	- 10 -
Figure S9: Geometry of the PTP-CHO building block, optimized on PBE0-D3/def2-TZVP level of theory. Representative dihedral angles are marked in red.....	- 11 -
Figure S10: Geometries of the N_x building block units optimized on PBE0-D3/def2-TZVP level of theory. Representative dihedral angles are marked in red.....	- 12 -
Figure S11: HOMO and LUMO of the PTP-CHO building block obtained at PBE0/def2-TZVP level of theory.....	- 12 -
Figure S12: HOMO and LUMO of the N_x building block units obtained at PBE0/def2-TZVP level of theory.....	- 13 -
Figure S13: Orbital energies and Kohn-Sham Band-Gaps for the PTP-CHO building block in comparison with the N_x building block units, all data obtained at PBE0/def2-TZVP level of theory.....	- 13 -
Figure S14: Comparison of Kohn-Sham Band-Gaps and excitation energies on PBE0/def2-TZVP and TD-PBE0/def2-TZVP level of theory.....	- 13 -
Figure S15: Spin densities of the vertical radical anion for the PTP-CHO building block and the N_x building block units, calculated on PBE0-D3/def2-TZVP level of theory.....	- 14 -
Figure S16: 300 MHz ^1H NMR of 2 in CDCl_3	- 15 -
Figure S17: 75 MHz ^{13}C NMR of 2 in CDCl_3	- 15 -
Figure S18: 300 MHz ^1H NMR of 3 in CDCl_3	- 16 -
Figure S19: 75 MHz ^{13}C NMR of 3 in CDCl_3	- 16 -
Figure S20: 300 MHz ^1H NMR of 5 in CDCl_3	- 17 -
Figure S21: 75 MHz ^{13}C NMR of 5 in CDCl_3	- 17 -
Figure S22: 300 MHz ^1H NMR of PTP-CHO in CDCl_3	- 18 -

Table S1: Parameters of Rietveld refinement

	PTP-COF
Restraints & constraints	$a=b\neq c$; $\alpha=\beta=90^\circ$, $\gamma=120^\circ$.
Rwp	1.833
a (Å)	27.7(8)
b (Å)	27.7(8)
c (Å)	3.55
α (°)	90
β (°)	90
γ (°)	120

Table S2: Dihedral angles in PTP-CHO and N_x -CHO building blocks obtained from optimized geometries on the PBE0-D3/def2-TZVP level of theory. Dihedral angles are reported in a clockwise order, starting from the upward pointing ligand A. Structures of the respective aldehydes can be found in Figure 1.

	Dihedral Angle [°]			
	A	B	C	Average
PTP-CHO	16.3	16.3	-18.4	17.0
N_0-CHO	39.1	39.1	39.1	39.1
N_1-CHO	39.1	24.2	26.2	29.8
N_2-CHO	7.5	24.4	24.5	18.8
N_3-CHO	0.0	0.0	0.0	0.0

Table S3: Radiative and non-radiative rates of PTP-COF under different experimental conditions

Sample	Φ^a	τ , ns (amplitude)	$\langle\tau\rangle^b$, ns	$k_r (\times 10^7 \text{ s}^{-1})^c$	$k_{nr} (\times 10^8 \text{ s}^{-1})^d$
Solid sample	0.0415	0.32 (10.58%), 1.13 (58.2%) and 3.54 (31.22%)	1.8	2.306	5.325
Water dispersion	0.0209	0.1 (9.73%), 0.57 (44.28%) and 1.55 (45.99%)	0.97	2.155	10.094
Photocatalytic conditions	0.0087	0.09 (14.86%), 0.37 (51.02%) and 1.07 (34.13%)	0.57	1.526	17.391

Φ - Quantum yield; τ - Fluorescence lifetime fitted to three exponentials; $\langle\tau\rangle$ - Amplitude-weighted average lifetime;

k_r - radiative rate; k_{nr} - non-radiative rate.

^a $\lambda_{exc}=380$ nm; ^b $\langle\tau\rangle = \sum a_i \tau_i / \sum a_i$; ^c $k_r = \Phi / \tau$; ^d $k_{nr} = (1 - \Phi) / \tau$

Table S 4: Excitation energies for the PTP-CHO building block unit calculated on TD-PBE0/def2-TZVP level of theory.

	State	Excitation Energy [eV]	Oscillator Strength [km/mol]	Occupied Orbital	Virtual Orbital	Orbital Contribution [%]
PTP-CHO	6	4.06	0.8081	HOMO	LUMO+1	40.5
N₀-CHO	5	4.30	0.7813	HOMO	LUMO	33.2
N₁-CHO	5	4.22	0.5047	HOMO	LUMO+1	90.4
N₂-CHO	7	4.25	0.5450	HOMO	LUMO+1	81.7
N₃-CHO	9	4.24	0.4739	HOMO-4	LUMO+1	28.1

Table S5: Calculated vertical radical stabilization energies as differences in total energies between radical anionic, radical cationic and neutral states of the PTP-CHO model system, PBE0-D3/def2-TZVP level of theory.

	Radical Cation				Neutral
	ΔVCSE [eV]	ΔVCSE [H]	VCSE [H]	Total Energy [H]	Total Energy [H]
PTP-CHO	-0.53	-0.01935494	0.30533824	-1312.19120015	-1312.49653838
N0-CHO	-0.52	-0.01928853	0.30540465	-1264.09669101	-1264.40209566
N1-CHO	-0.55	-0.02013946	0.30455372	-1280.13258163	-1280.43713535
N2-CHO	-0.34	-0.01231277	0.31238041	-1296.16429579	-1296.47667619
N3-CHO	0.00	0.00000000	0.32469318	-1312.19606741	-1312.52076059

	Radical Anion				Neutral
	ΔVASE [eV]	ΔVASE [H]	VASE [H]	Total Energy [H]	Total Energy [H]
PTP-CHO	0.34	0.01253149	-0.05811023	-1312.55464862	-1312.49653838
N0-CHO	0.59	0.02161944	-0.04902228	-1264.45111794	-1264.40209566
N1-CHO	0.32	0.01176033	-0.05888139	-1280.49601674	-1280.43713535
N2-CHO	0.12	0.00442453	-0.06621719	-1296.54289338	-1296.47667619
N3-CHO	0.00	0.00000000	-0.07064172	-1312.59140231	-1312.52076059

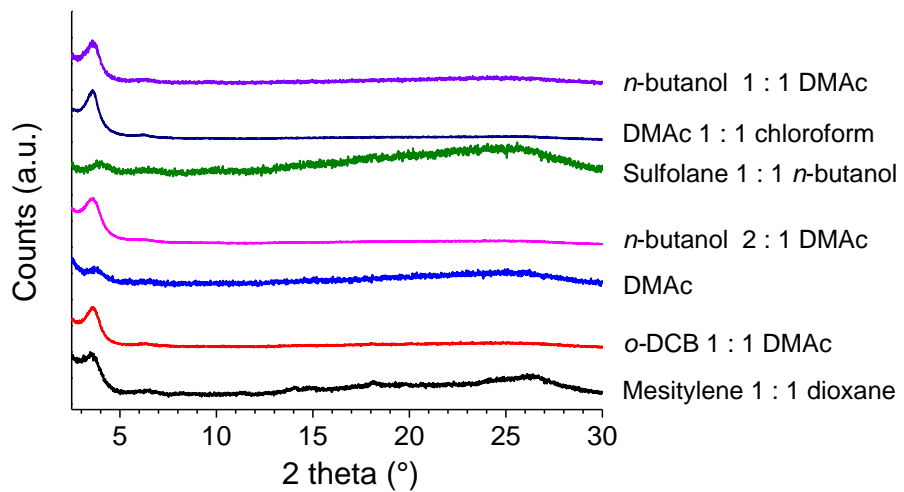


Figure S1: XRPD of PTP-COF synthesized in different solvent systems. DMAc = dimethyl acetamide, *o*-DCB = *o*-dichlorobenzene.

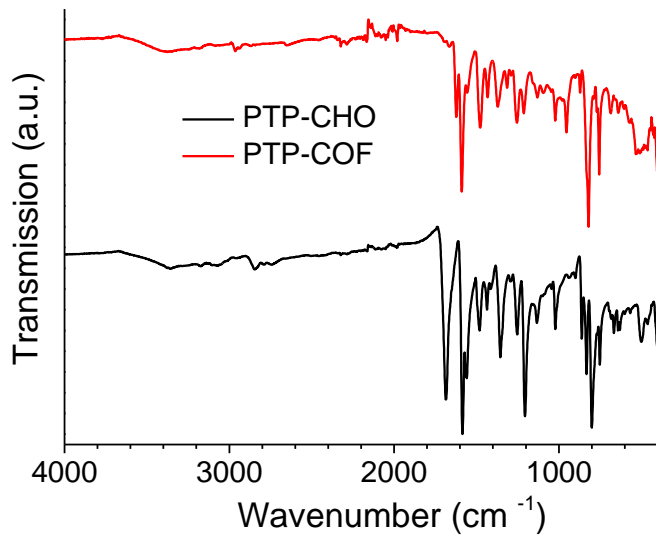


Figure S2: Full IR Spectrum of PTP-CHO and PTP-COF.

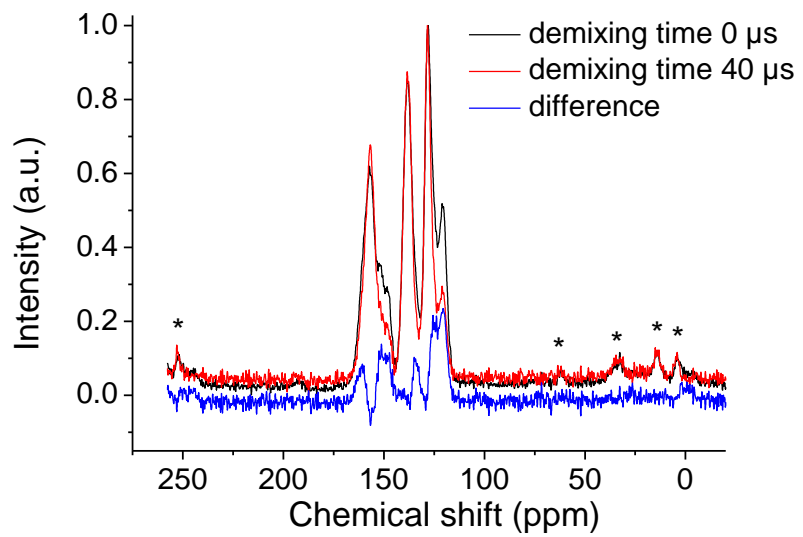


Figure S3: ^{13}C ssNMR of PTP-COF. Asterisks denote spinning side bands.

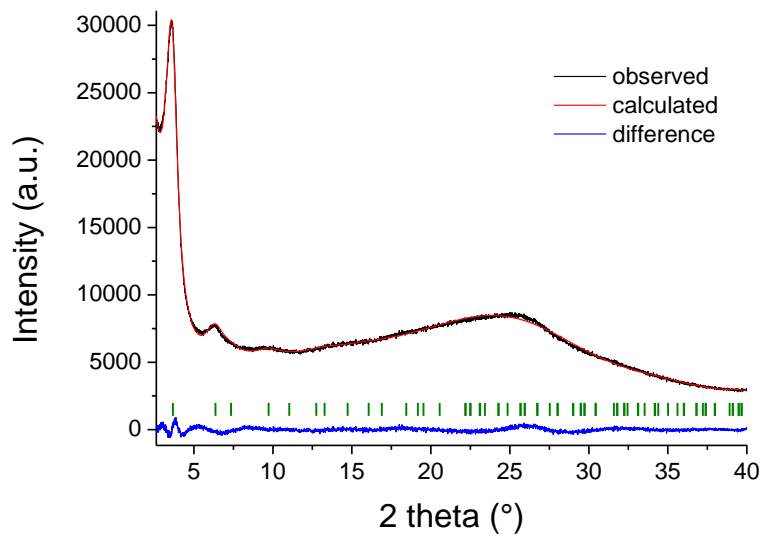


Figure S4: Rietveld refinement of the PTP-COF shows a good fit to the experimentally observed powder pattern (R_{wp} : 1.833)

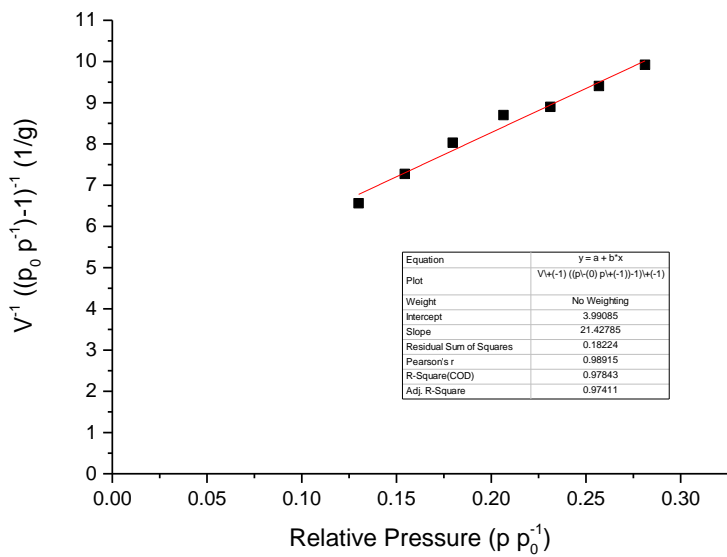


Figure S5: BET fit of the surface area of PTP-COF.

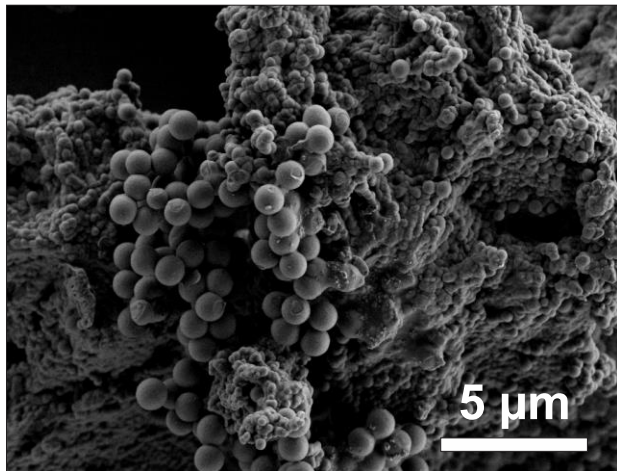


Figure S6: SEM image of the PTP-COF showing the spherical particles and the intergrown agglomerates.

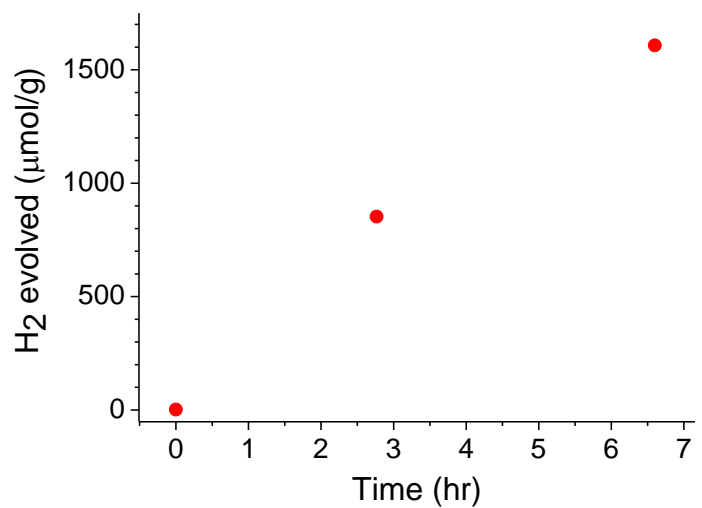


Figure S7: Hydrogen evolution under full spectrum light.

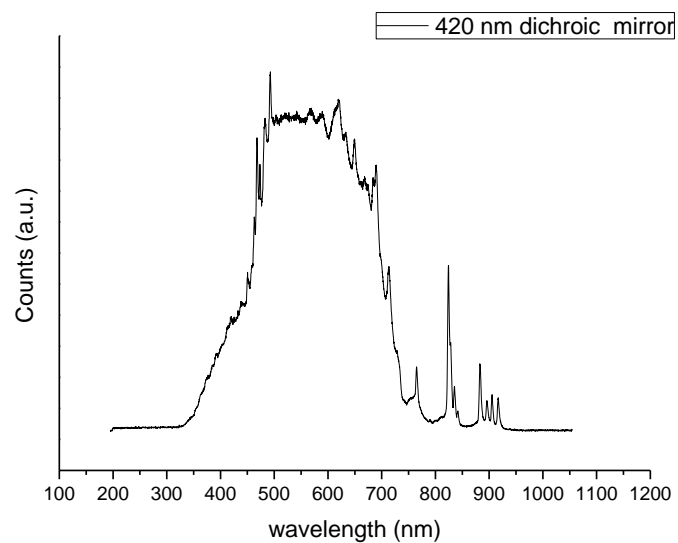


Figure S8: Spectrum of the xenon lamp with the dichroic mirror used for the AM1.5 photocatalysis experiments.

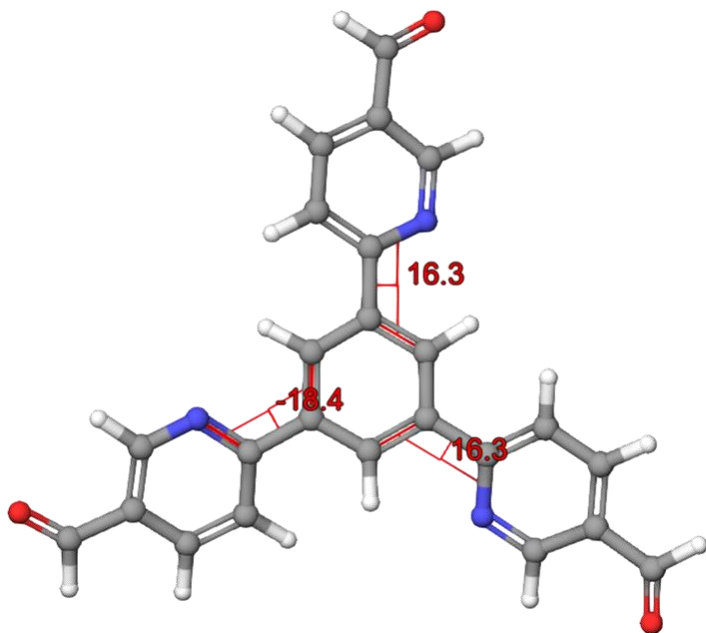
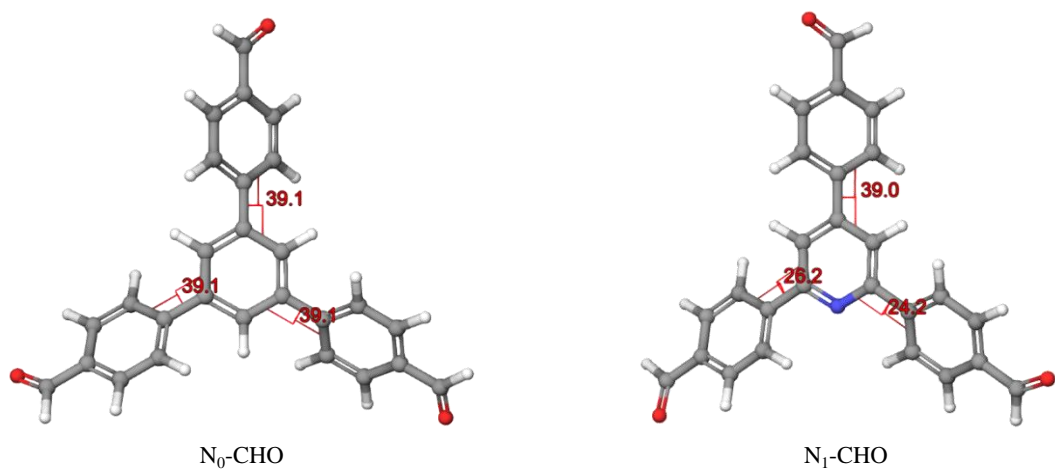


Figure S9: Geometry of the PTP-CHO building block, optimized on PBE0-D3/def2-TZVP level of theory. Representative dihedral angles are marked in red.



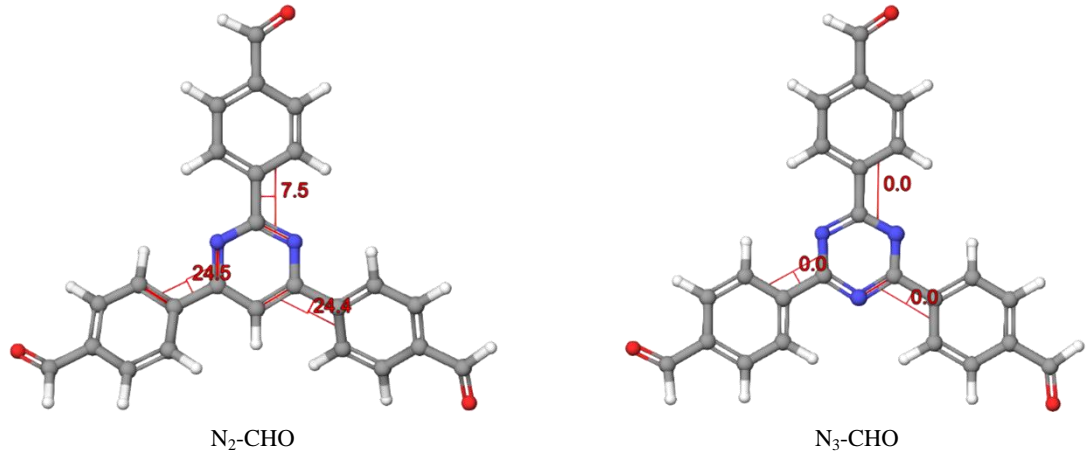


Figure S10: Geometries of the N_x building block units optimized on PBE0-D3/def2-TZVP level of theory. Representative dihedral angles are marked in red.

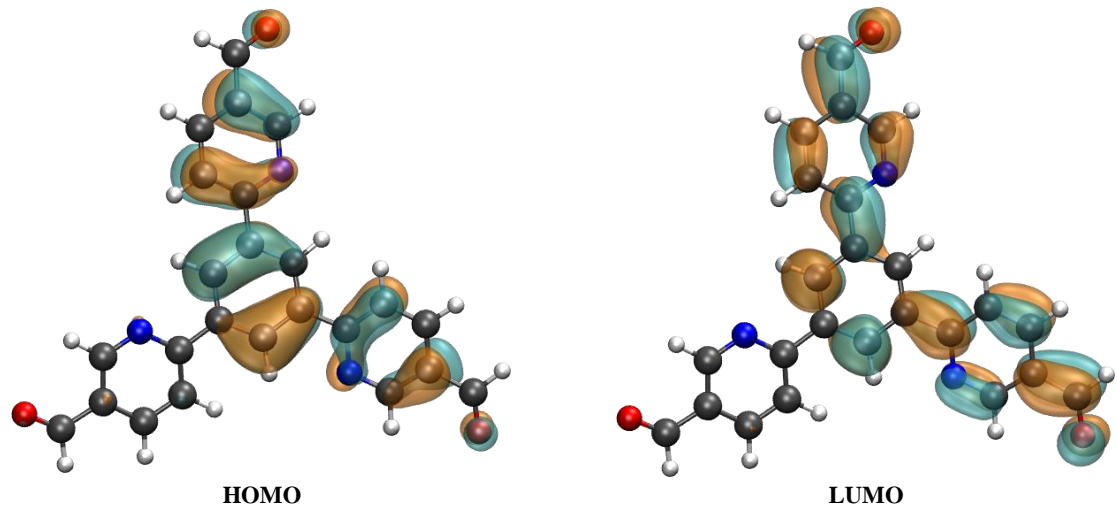


Figure S11: HOMO and LUMO of the PTP-CHO building block obtained at PBE0/def2-TZVP level of theory.

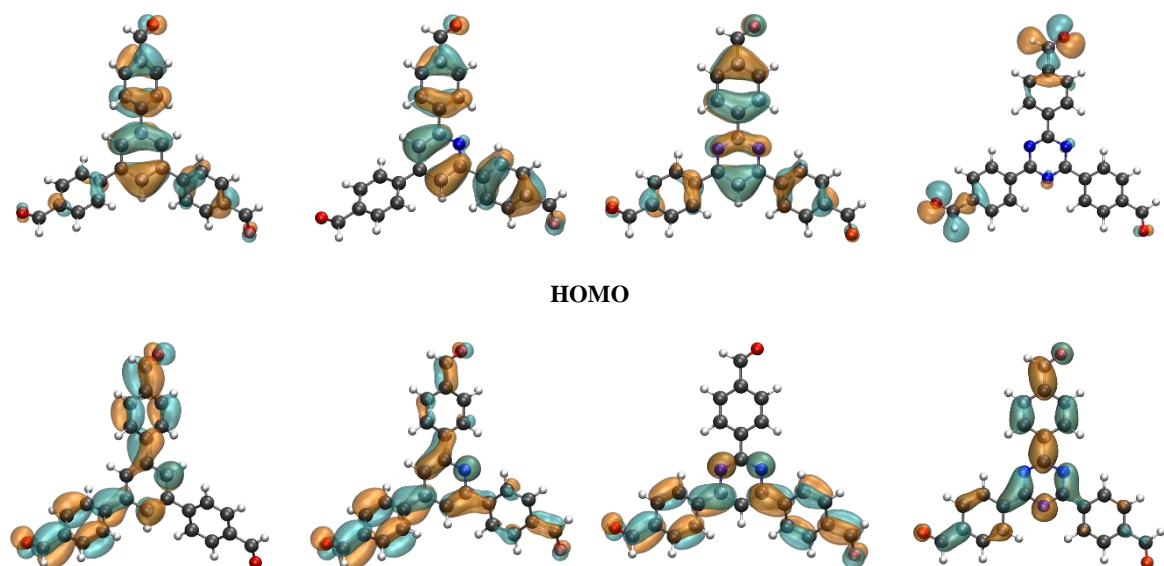




Figure S12: HOMO and LUMO of the N_x building block units obtained at PBE0/def2-TZVP level of theory.

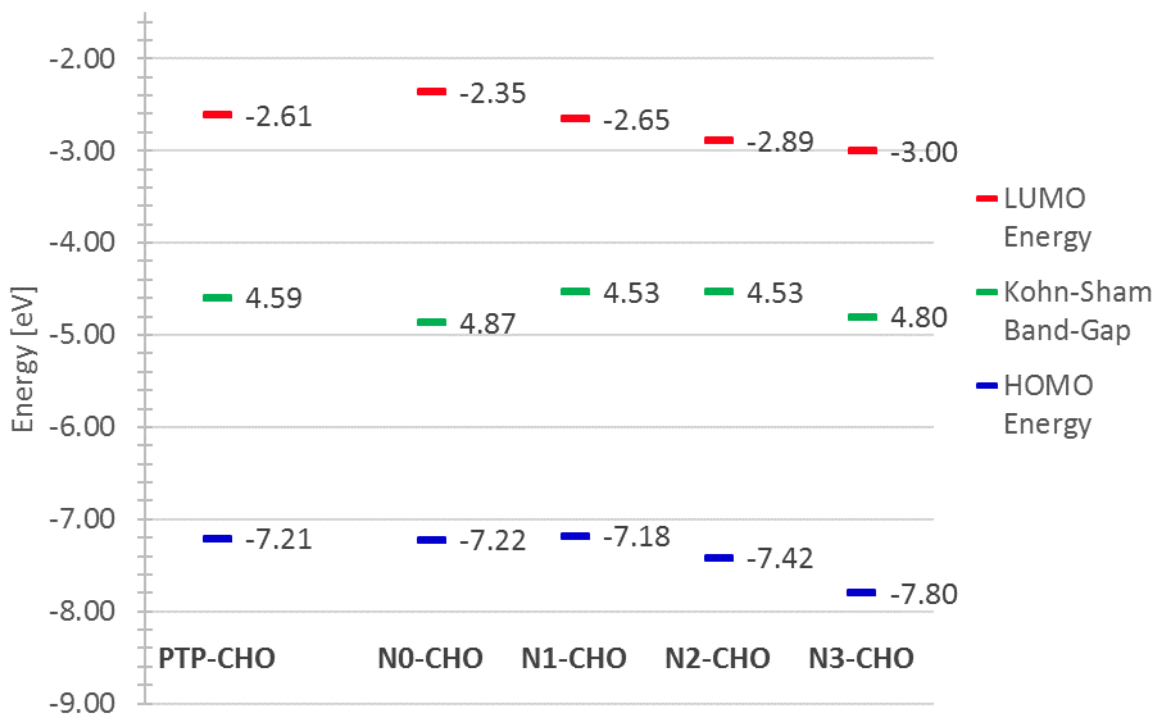


Figure S13: Orbital energies and Kohn-Sham Band-Gaps for the PTP-CHO building block in comparison with the N_x building block units, all data obtained at PBE0/def2-TZVP level of theory.

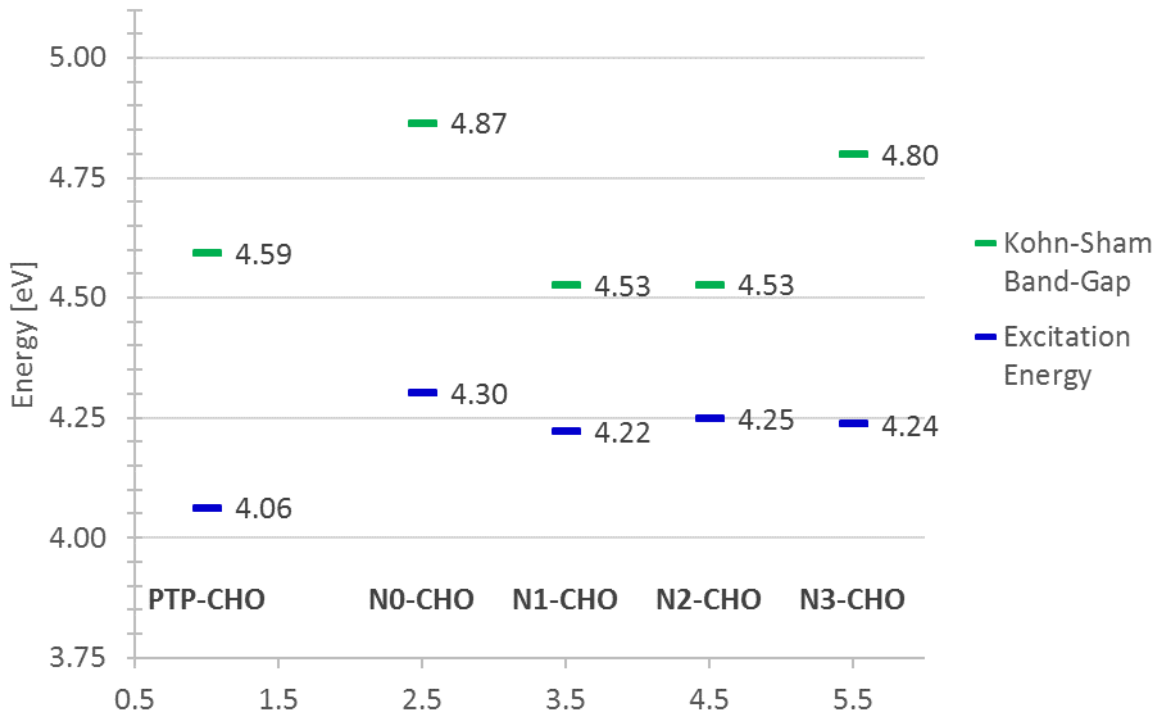


Figure S14: Comparison of Kohn-Sham Band-Gaps and excitation energies on PBE0/def2-TZVP and TD-PBE0/def2-TZVP level of theory.

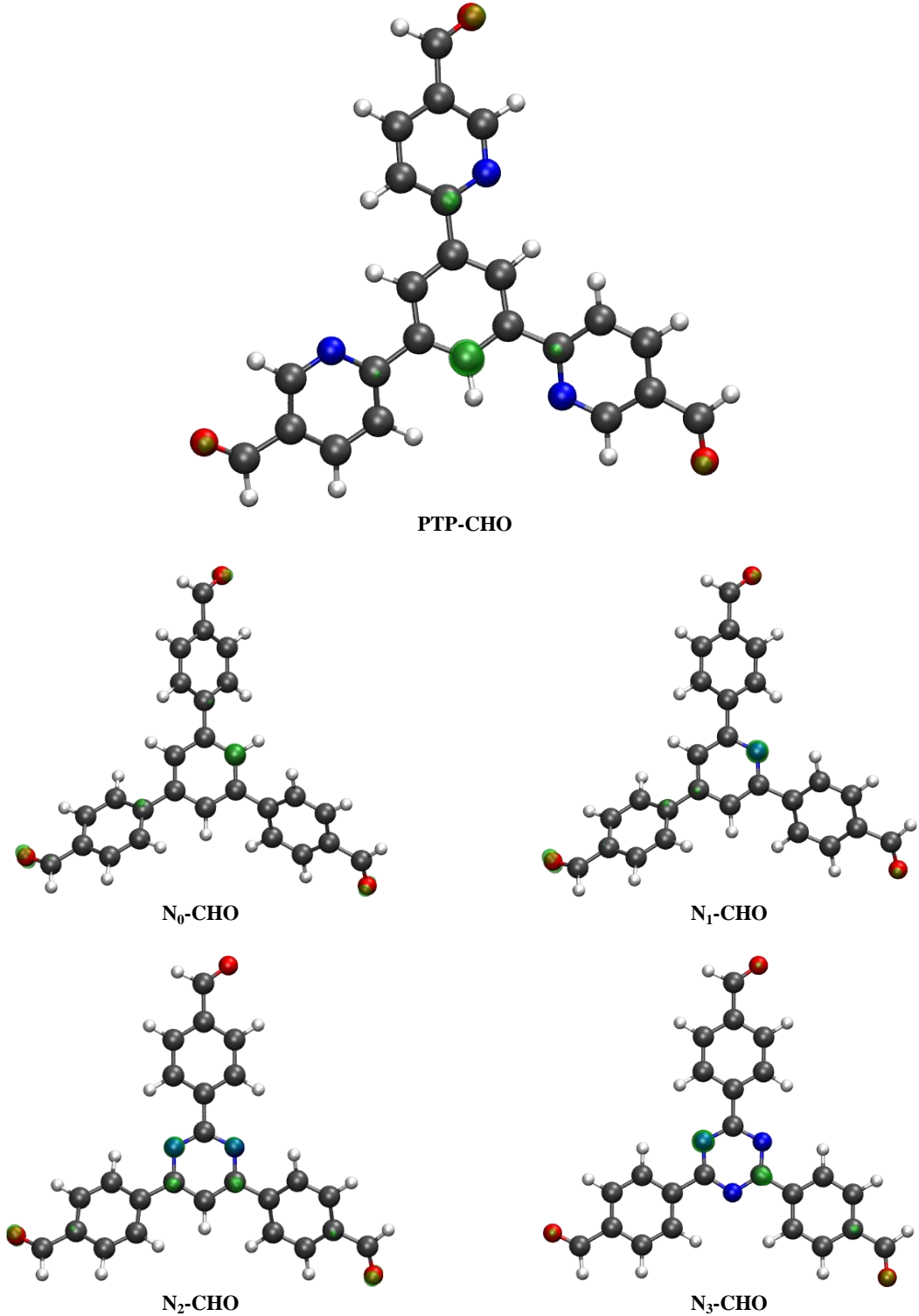


Figure S15: Spin densities of the vertical radical anion for the PTP-CHO building block and the Nx building block units, calculated on PBE0-D3/def2-TZVP level of theory.

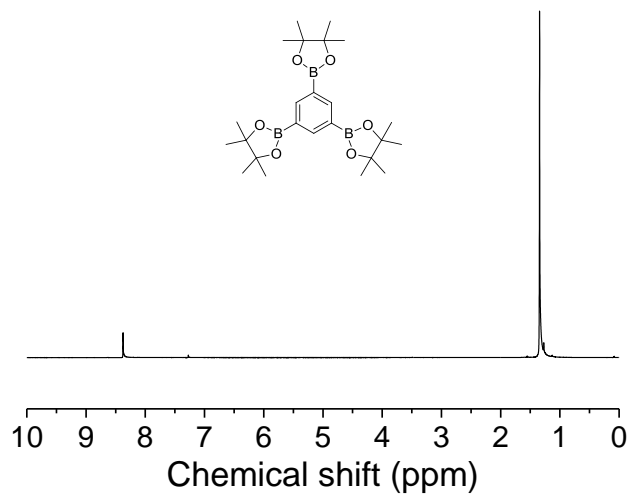


Figure S16: 300 MHz ^1H NMR of **2** in CDCl_3 .

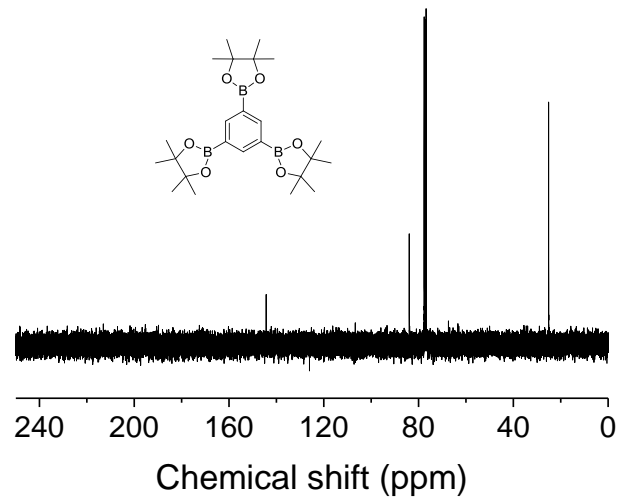


Figure S17: 75 MHz ^{13}C NMR of **2** in CDCl_3 .

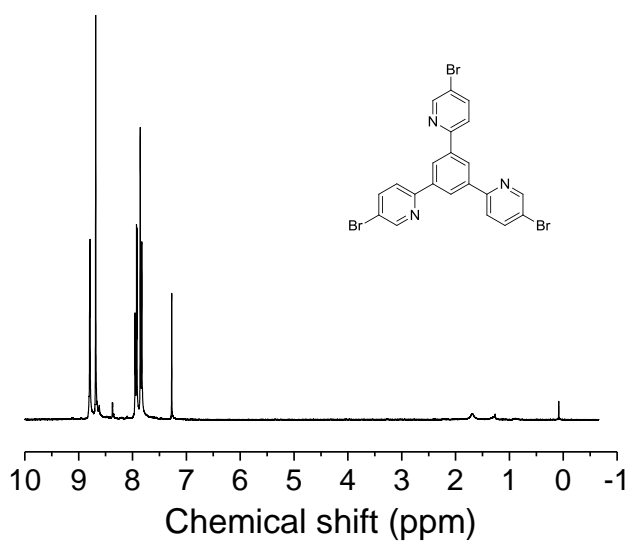


Figure S18: 300 MHz ^1H NMR of **3** in CDCl_3 .

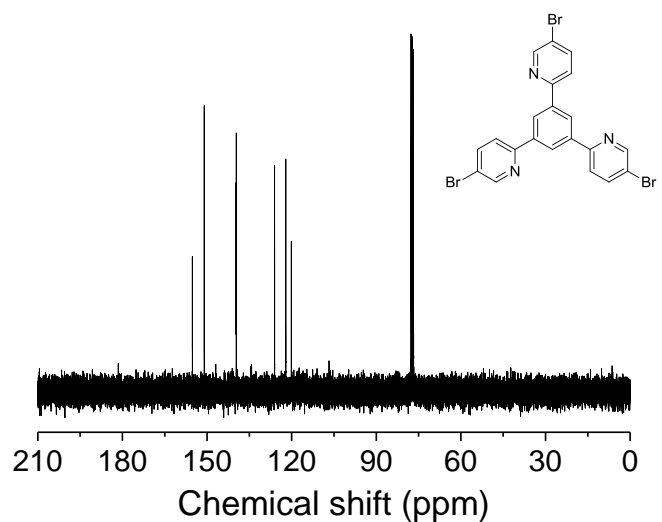


Figure S19: 75 MHz ^{13}C NMR of **3** in CDCl_3 .

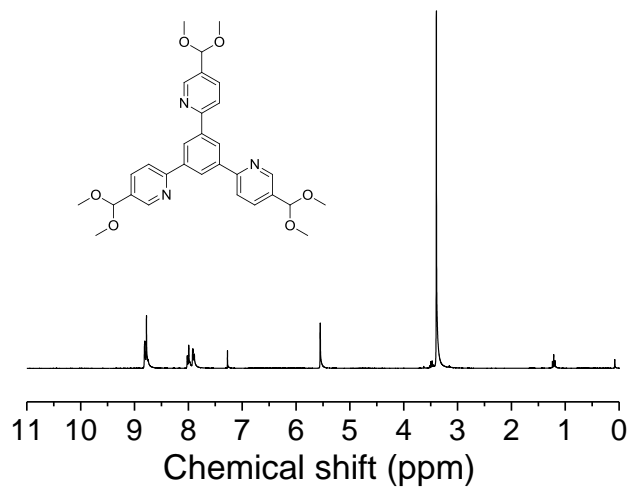


Figure S20: 300 MHz ^1H NMR of **5** in CDCl_3 .

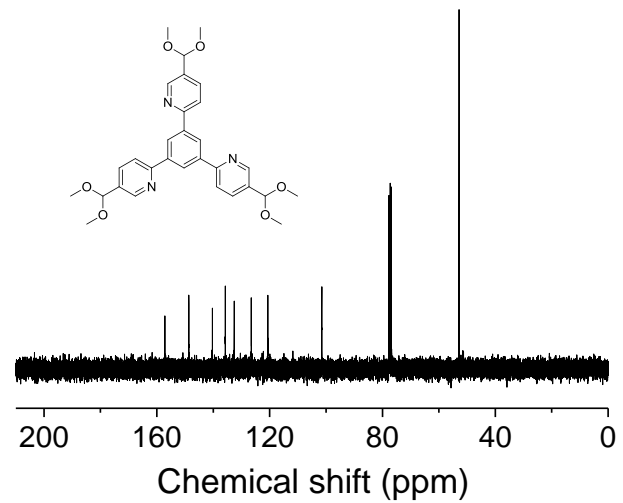


Figure S21: 75 MHz ^{13}C NMR of **5** in CDCl_3 .

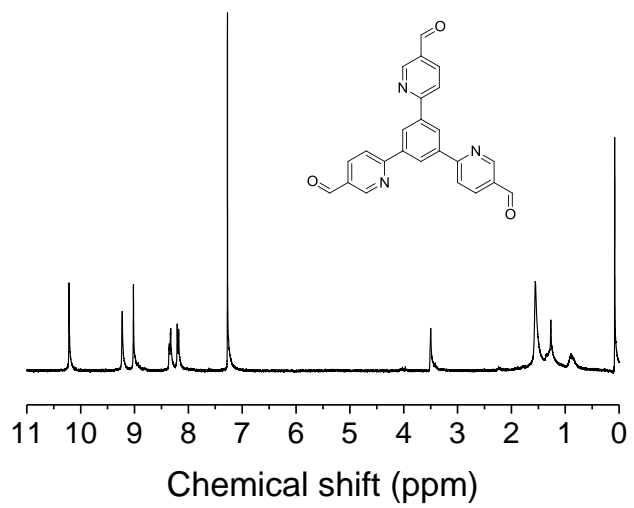


Figure S22: 300 MHz ^1H NMR of PTP-CHO in CDCl_3 .